Thermally-oxidized aluminum as catalyst-support layer for vertically-aligned single-walled carbon nanotube growth using ethanol

Mohd Asyadi Azam [a, *], Akihiko Fujiwara [b], Tatsuya Shimoda [a]

[a] School of Materials Science, Japan Advanced Institute of Science and Technology (JAIST), 1-1 Asahidai, Nomi, Ishikawa, 923-1292 Japan

[b] Research and Utilization Division, Japan Synchrotron Radiation Research Institute (JASRI), 1-1-1, Kouto, Sayo-cho, Sayo, Hyogo 679-5198 Japan

* Corresponding Author: asyadi@jaist.ac.jp (Mohd Asyadi Azam)

Tel: +81-761-51-1553

Fax: +81-761-51-1149

Abstract

Characteristics and role of Al oxide (Al-O) films used as catalyst-support layer for vertical growth of single-walled carbon nanotubes (SWCNTs) were studied. EB-deposited Al films (20 nm) were thermally-oxidized at 400 ^{o} C (10 min, static air) to produce the most appropriate surface structure of Al-O. Al-O catalyst-support layers were characterized using various analytical measurements, i.e., atomic force microscopy (AFM), X-ray photoelectron spectroscopy (XPS), and spectroscopy ellipsometry (SE). The thermally-oxidized Al-O has a highly-roughened surface, and also has the most suitable surface chemical states compared to other type of Al-O support layers. We suggest that the surface of thermally-oxidized Al-O characterized in this work enhanced Co catalyst activity to promote the vertically-aligned SWCNT growth.

1. Introduction

For the realization of functional products using single-walled carbon nanotube (SWCNT), such as field-emitter arrays, transistors and capacitors, reconstructing and aligning the SWCNTs into desired structures was found to be extremely difficult. Aligned SWCNT arrays on substrates offer advantages for a wide variety of in-demand applications, compared to those with random and entangled forms of CNTs that require modification or adjustment. Various methods have been developed to grow vertically-aligned (VA-) SWCNTs. Among them, the alcohol catalytic chemical vapor deposition (ACCVD) method [1 – 3] is popular for its economical merit, wide selectivity of substrates, and better catalytic reaction. In CNT growth using ACCVD technique, several groups have succeeded in growing VA-SWCNTs by controlling various experimental conditions [4 – 6].

Regardless of the growth method, CNT formation strongly depends on catalytic activity and catalyst lifetime [7, 8]. The literature has been presenting the functions and advantages of catalyst-support materials, especially the metal oxide layer. Among them, aluminum oxide (Al-O), including alumina (Al_2O_3) is said to have appropriate surface condition (physically and/or chemically) to support metal catalyst nanoparticles for well-organized CNT growth. Physical interactions are attributed to the size of metal particles, due to its porous support [9], to the surface roughness which can provide more active CNT nucleation sites [10], and also to the effects of crystallographic structure of both catalyst and support material [11]. Highly-roughened and/or porous support surface also may affect the CNT growth, by trapping the catalysts' particles and makes the catalyst permeable to hydrocarbon molecules, so that feed gas/vapor reaches the catalyst at a higher rate [12]. Chemical interactions involve charge transfer between support and catalyst. This charge transfer is correlated to the Lewis base or acid character of the support [9].

Several methods were introduced to directly prepare Al-O support material. These include sputter deposition [13], electrochemical approach for anodic aluminum oxidation (AAO) [14], sol-gel [15], etc. It was also reported that a two-step synthesis method, namely, deposition and oxidation of deposited Al films, can produce appropriate Al-O surface to support the catalyst for VA-SWCNT growth. Noda *et al.* in ref. [4] discussed SWCNT growth performance using Co catalyst by comparing SiO_2 and air- oxidized Al-O underlayers. They also claimed air-oxidized Al-O was preferable for SWCNT growth performance, compared to the directly-deposited alumina underlayer [16]. Furthermore, amorphous Al-O produced by thermal oxidation in air was preferable to single-crystalline sapphire [6]. However, the surface analysis of air and/or thermally-oxidized Al-O films has not been well discussed. For example, when discussing different alumina underlayers for VA-CNT growth, Amama *et al.* mentioned that the variations in the surface chemical state of Al-O might contribute to the different catalytic behaviors [8].

In order to achieve optimum SWCNT growth rate, good understanding of the growth mechanism is required. Thus, it is critical to investigate the effects of each material layer/film produced on the substrate surface. In particular, the surface physical condition and chemical state of the support layer must be investigated, before exploring the catalyst activity. In this paper, we report the properties of Al films oxidized under various experimental conditions. The samples were analyzed by X-ray photoelectron spectroscopy (XPS), atomic force microscopy (AFM), and spectroscopic ellipsometry (SE). For discussion of the role of the Al-O films in VA-SWCNT growth, experimental results are compared using our established growth process.

2. Experimental

First, Si (100) wafer with thermal oxide layer (400 nm) was used as substrate. The substrates were rinsed with acetone, then in ethanol for 10 min cleaning using ultrasonic bath. The Al thin films of 20 nm nominal thickness were deposited using electron beam physical vapor deposition (EBPVD) at 10^{-4} Pa. The deposition rate was monitored by a quartz resonator and was kept constant at 0.1 nm sec^{-1}: The thickness monitor of quartz resonator was calibrated using Alpha-Step500 surface profiler and AFM. In order to discuss properties of Al-O support layers fabricated by different methods and their effects on CNT growth, we prepared five types of Al-based support layers on SiO_2/Si substrates. Four samples were prepared using deposited Al films on SiO_2/Si substrates and among them, three were fabricated by different post-oxidation treatments of the Al films. The oxidation methods were thermal, ultra-violet ozone (UVO) and plasma oxidation. Another sample was a directly-deposited of 20 nm alumina (different EBPVD source). We confirmed that temperature of substrate during EBVPD process was less than 200 ^{o} C, being low enough not to affect the morphology of films.

For the formation of thermally-oxidized Al-O, deposited Al was first naturally-oxidized at room temperature for 2 hours. Then, the substrate was subsequently transferred to CVD reactor used for CNT growth, and oxidized at T_{to} = 400 ^{o} C in static air for 10 min (Al-T). For UVO oxidation, the sample was exposed to UVO for 60 min (Al-UV). For plasma oxidation, treatment was performed under conditions of radio frequency (RF) power at 30 W, oxygen flow rate of 50 sccm for 10 min (Al-P). Note that the optimization of treatment conditions for each sample was performed accordingly. All Al-O films were characterized by tapping mode AFM (Seiko Instruments Inc.) and XPS (Fison Instruments S-PROBE ESCA). XPS measurements were performed with Al Kα (1486.6 eV) as the X-ray source and the samples were analyzed at 90 ^{o} take-off angle to the surface. The photoelectron binding energy (BE)

was calibrated using C 1s narrow spectrum, at 284.6 eV, and chamber pressure during the measurement was 10^{-7} Pa. As-deposited Al films were also characterized by the same methods as a reference (Al). Table 1 shows the overview of all samples.

For CNT growth, Co catalyst (0.5 nm nominal thickness) was consequently deposited on top of Al films using the same EBPVD, and then followed by the oxidation process of Al films. It is important to note that Co deposition on Al films before or after oxidation process of Al-O support layer produced qualitatively the same results, within experimental error of CNT growth results. Electric furnace (MILA-3000) was employed as the CVD reactor. Ar/H_2 (3% H_2) as the pretreatment gas was supplied into the reactor at a pressure of 0.4 kPa concurrently with 4 min rapid ramping of the furnace. The Ar/H_2 gas continuously flowed after the furnace temperature reached the CVD temperature (T) of 750 ^{o}C for further 5 min annealing process. Then, the mixed gas flow was stopped, and then ethanol vapor was immediately introduced into the furnace at flow rates of 110 – 130 sccm. The internal pressure and CVD processing time were fixed at 3 kPa and 10 min, respectively. The CNTs grown from Co/Al-O support layers were characterized by scanning electron microscopy (SEM; Hitachi S-4100) and Raman spectroscopy (Tokyo Instruments; Nanofinder 30) with λ = 632.8 nm (HeNe).

For comparison and clarity, Al-T sample coated with 0.5 nm Co (Co/Al-T) was also characterized. Detailed surface chemical states of Co/Al-T were investigated by means of XPS analysis. Also, the effect of thermal oxidation (400 ^{o}C, air) for 10 min and further annealing at T_{CVD} (750 ^{o}C, Ar/H_2) for 5 min to Al-T surface were investigated using AFM and variable angle spectroscopic ellipsometry (VASE; J.A.Woollam Co. Inc.) with λ = 350 – 1000 nm and 75 ^{o} incident angle. Results obtained by VASE were analyzed using WVASE32 software.

3. Results and discussion

3.1 Characteristics of various Al-based support layers and CNT growth from them

First, we discuss surface properties of Al, alumina, and Al-O support layers fabricated by different oxidation methods. Figure 1(a) shows the AFM tapping mode images of all samples; root mean square (RMS) surface roughness and grain size estimated by AFM images are summarized in Table 1. It was found that each oxidation method produced different surface morphological structures. Al-T has relatively high RMS surface roughness, which is almost the same as that of Al films, followed by Al-UV, Al-P, and alumina. The value of RMS surface roughness shows the same tendency as the samples' mean grain size determined by the AFM image height direction. XPS was performed to investigate the surface composition of all samples.

Detailed XPS measurement results of all samples are shown in Figure 1(b). Al metal (72.0 eV) and Al oxide (75.0 eV) signals were separated for Al, Al-T, Al-UV, and Al-P samples by fitting with Gauss functions (software S-Probe 1.36.00) to the XPS profiles at Al 2p region. As shown in the figure, peak fitting for all samples (except alumina) resulted in Al 2p oxide (blue line), Al 2p interface (green), Al $2p_{1/2}$ (grey), and Al $2p_{3/2}$ (metal; red) peaks [17]. The Al metal to oxide ratios, I_{metal}/I_{oxide} were calculated from the integrated intensity of each peak (Table 1). This is important for the indication of oxide structure of prepared Al-O support layers. Al-P sample produced the lowest I_{metal}/I_{oxide} ratio, followed by Al-T, Al-UV, and Al. Significantly high Al oxide signal and the absence of Al metal signal for as-deposited alumina sample confirms that metal was not present in the sample composition, thus the I_{metal}/I_{oxide} ratio was described as 0. Unlike other samples, high intensity of Al $2p_{3/2}$ spectrum at 72.0 eV reveals the presence of pure metal on non-treated Al sample surface.

By using various support layers, ACCVD growth process was performed to Co (0.5 nm)/Al or Al-O (20 nm)/SiO_2/Si substrates, and the SEM images of grown CNT on the substrates are shown in Figure 2(a). CNT from Co/Al-T sample produced the tallest CNT forests, followed by Co/Al-UV and Co/Al-P. However, VA-CNT growth was not promoted for Co/Al and Co/alumina samples. The CNTs were randomly-grown on these two types of substrates. In a previous study, we also confirmed that tangled "spaghetti-like" (non-aligned) SWCNTs were grown without the supporting layer (Co on SiO_2/Si) [3]. In the case of Co/alumina sample, the CNTs were agglomerated and formed ~3-μm thickness CNT carpet. The VA-CNT height describes the growth rate of the CNTs in CVD-based growth system [18]. Therefore, the VA-CNT growth was well-promoted by using thermal, UVO and plasma treated Al-O support layers. Figure 2(b) plots the relation between VA-CNT height and RMS surface roughness of different support layers. It was found that the CNT height and support layer's surface roughness show a good agreement, except for pure Al. The rougher the support layer surface is, the better growth rate can be achieved.

In the case of non-treated Al support layer, although the RMS surface roughness was high and comparable to Al-T, VA-growth was not promoted at all. This might be attributed to the differences in surface chemical states of the samples.

By taking account of CNT growth efficiency on all substrates, low Al oxide composition and very low surface roughness somehow impeded the CNT growth performance. The results suggested that low Al metal (or high Al oxide) composition ratio ($I_{metal}/I_{oxide} < 0.2$) and high RMS surface roughness (> 3 nm) of Al-O layers are essential for VA-CNT growth. One of our results, the importance of surface morphology of Al-O as catalyst-support in growing VA-CNTs, is consistent with the report by Delzeit *et al.* [10]. Surface roughness was reported may hinder surface diffusion of the catalyst inward support surface and thus its coalescence into (too) large particles. From above, different catalyst-support surface

roughness will determine Co catalyst diffusion behavior (diffusion coefficient). The surface diffusion rate of a specific atom on a substrate depends not only on the substrate nature but also on its roughness [19]. Even if the catalyst-support surface is highly-roughened or highly-porous, large contact area with the catalyst is also essential to accelerate CNT growth. Here, we propose that thermal oxidation of EB-deposited Al support increases its surface roughness, thus providing more active nucleation sites. Further, from different Al-O chemical states (originated from surface oxidation states), significant variations in CNT growth results are suggested to be due to the alteration of Co catalyst electronic structure. The Co electronic density of states associated with Al-O surface atoms might be altered at Al-O surface. Related to the basis of metal-support interaction, electronic interaction between metal catalyst particle and support layer greatly affects the CNT yield and structure [9]. It is therefore can be suggested that Co catalyst activity is strongly depends on Al-O physical structures and surface chemical states. The surface morphology and composition (surface chemical states) of Al-O films are important in understanding their role in promoting VA-SWCNT growth.

Uniform VA-growth of more than 60-μm height was confirmed from Co/Al-T sample. SEM images (Figure 3(a)) show the vertical alignment of CNTs perpendicular to the substrate, where most of the area of the substrate was covered by VA-CNTs. On the other hand, the peaks at the radial breathing mode (RBM) region in the Raman spectrum in Figure 3(b) verified that those forests were composed of SWCNTs [20]. Thermal oxidation of EB-deposited Al films was effective for the growth of VA-SWCNTs on any kind of substrates, including electrically-conducting foil for use in electrochemical capacitors [21, 22]. The detailed characteristics of thermally-oxidized Al-O will be discussed in the next section.

3.2 Details of thermally-oxidized Al-O catalyst-support layer

3.2.1 Surface chemical states (with and without Co catalyst)

Most significant characteristics of thermally-oxidized Al-O (Al-T) were elaborated from the XPS and AFM. XPS *ex-situ* analysis was performed to investigate the surface chemical states of sample Al-T. The changes experienced by Al surface from the behavior of the Al 2p doublet were measured. For the first approximation, Figure 4(a) shows the typical survey spectrum of Co/Al-T and Al-T sample after being heat-treated at 400 ^{o} C, in air. The blank SiO_2/Si substrate was measured as reference. Co 2p and Co 3p peaks were clearly observed at around 800 and 65 eV for the sample coated with 0.5 nm Co catalyst. From survey spectra, Al-T surface (with and without Co) contributed 3 main photoelectron signals; Al 2p, C 1s, and O 1s. Importantly, for both Al-T and Co/Al-T samples, no photoelectron intensity was reflected from the SiO_2 underlayer; the absence of Si signals confirmed the uniformity of Al and Co films.

Figure 4(b) depicts the XPS narrow spectra of O 1s and Al 2p regions for three types of Al-T samples (without Co). As-deposited and thermally-oxidized samples are the same as Al and Al-T in Figure 1(b), respectively. Sample treated at CVD growth temperature (T_{CVD}) with Ar/H_2 was also investigated (further-annealed). The original Al metal peak is at 72.0 eV, and the representative spectrum of Al oxide was confirmed at 75.0 eV. Full width at half maximum (FWHM) of 2.3 eV (broad, > 2 eV) might explain the amorphous-like morphology of the films [23]. The chemical states of as-deposited Al changed with the different heating (oxidation and annealing) processes. The signal of Al metal decreased after 400 ^{o} C thermal oxidation (in air, *vacuum* off) and completely disappeared after further annealing at 750 ^{o} C (Ar/H_2, 0.4 kPa). The increase of Al oxide and O 1s intensities was also confirmed. These results indicate that most of the Al films were oxidized before the CVD growth process. In the case of Fe/alumina, Fe metal transforms to Fe_2O_3 during annealing, and remains on the sample surface, providing a situation where CNT growth is very efficient [24]. Therefore, it is

crucial to clarify the surface chemical states of Co on top of thermally-oxidized Al-O just before ethanol introduction for VA-SWCNT growth.

Figure 4(c) shows the XP spectra of the Al sample coated with 0.5 nm Co catalyst films (Co/Al-T). The Co 2p spectra were normalized at the maximum intensity in order to facilitate comparison. Since all spectra were collected under the same measurement conditions, the intensities of all signals indicate a direct measure of the degree of Co dispersion. For Al 2p region, as compared to a sample without Co, the increase of Al oxide intensity is similar. However, no Al metal signal was observed for thermally-oxidized sample, and Al 2p signal intensity of all samples showed a slight decrease, which may have been influenced by Co catalyst films on the surface. Next, we discuss important findings from XPS measurement at Co 2p regions. First, main signals of Co 2p region came from 781 eV (Co $2p_{1/2}$) and 797 eV (Co $2p_{3/2}$). The main signals of the Co $2p_{1/2,\ 3/2}$ doublet are separated by 16 eV. The peaks exhibit a shoulder at their high-energy side, the so-called shake-up satellite peak [25]. The shake-up satellite peak was used as a fingerprint for the recognition of high-spin Co(II) species in CoO compounds [26, 27]. The BE values of the Co 2p did not allow a clear distinction between CoO and the further-oxidized state, Co_3O_4 [$Co^{II}Co^{III}{}_2O_4$]. Therefore, shake-up satellite peaks (marked with an asterisk * in the figures) were essential to distinguish Co oxidation states in the as-deposited and 400 ^{o} C heat-treated (oxidized) samples. For as-deposited Co/Al, CoO originated from a common Co oxidation state, Co(II) (or Co^{2+}) was present on the sample surface. Relative intensity of the shake-up satellite peaks decreased after 400 ^{o}C heating in air (intentionally to oxidize Al films). Since the peak position of Co $2p_{1/2}$ and Co $2p_{3/2}$ remained at the same BE values, this indicates a transformation to a more oxidized state of CoO or further-oxidized to Co_3O_4.

After further-annealed at 750 ^{o} C (in Ar/H_2), Co catalyst was found remained in the state of Co oxide and peak of Co metal was not reflected. Since the samples were measured

by *ex-situ* XPS (exposed to air before measurement), atmospheric oxygen could easily re-oxidize metal particles due to the high dispersion and too small size of the Co. Co oxide might be reduced to Co metal, however, the re-formation of Co oxide due to air exposure is also definitely non-negligible. Although the absolute oxidation state of Co might be affected by the atmospheric oxygen, we discuss the difference of Co oxidation state by using relative relation between the samples since the samples were treated in the same way before XPS measurements, and measured under the same XPS condition within the system stability. XPS analysis of Co/Al-T demonstrates a preferred presence of CoO for all samples. Nevertheless, it is important that in this work, when Ar/H_2 gas not supplied during further annealing process, VA-SWCNT growth was not promoted (data not shown). Therefore, during ethanol introduction, the Co remains in the state of CoO and/or mixed with partially-reduced Co metal. Partial reduction of as-deposited CoO is conceivable and could be essential during further annealing process. In many cases of *in-situ* study, active state of the transition metal catalyst for CNT growth is metallic and CNTs are not nucleated from oxidized metal [28, 29]. The catalyst metal surface supplies sites to dissociate the hydrocarbon feedstock for the formation of carbon lattice and the liftoff of carbon cap.

The clear XPS peak reflection of Co oxide (no Co metal peak) strongly suggests the interaction (i.e. charge transfer process) between Al-O and Co occurred at the sample surface. The interaction between the catalyst and the support layer may vary the chemistry and morphology of the catalyst particles, thus resulting different CNT growth performance and characteristics [30]. This again indicates the importance of the surface chemical states of Al-O to the Co catalyst. Also, peaks in Co 2p region were drastically-decreased (magnified in the figure) and is agreed with catalyst-support analysis done by others [24, 28]. Here, a certain loss of Co 2p peak intensity can be attributed to several factors, i.e., aggregation of Co films to form nanoparticles, and/or Co association with Al-O. The BE values and the intensity

behavior of Co 2p for Co/Al-O in this work supported the possibility of partial (a minor) formation of the cobalt aluminate ($CoAl_2O_4$) [31]. To specifically and accurately conclude the surface chemical state of Co catalyst during VA-SWCNT growth, *in-situ* XPS could be the most ideal way and the best-practice analysis method. And importantly, the detailed nanostructure analysis of Co/Al-T (thermally-oxidized Al-O) sample used in this work is another interesting feature to be investigated.

3.2.2 Structure and surface morphology

From XPS measurements, sample surface oxide thickness, d (nm), can be estimated from the Al 2p I_{oxide}/I_{metal} ratio using the Equation (1);

$$d\ (\mathrm{nm}) = \lambda_{\mathrm{oxide}}\ \sin\theta \ln\left(\frac{N_{\mathrm{metal}}\,\lambda_{\mathrm{metal}}}{N_{\mathrm{oxide}}\,\lambda_{\mathrm{oxide}}}\frac{I_{\mathrm{oxide}}}{I_{\mathrm{metal}}}+1\right) \quad (1)$$

where the inelastic mean free path (IMFP) in the oxide, λ_{oxide} was 2.8 nm for Al-Kα–generated Al 2p photoelectrons emitted normal to the surface (θ = 90 ^{o}) of Al-O overlayer on Al [17]. The ratio of the volume densities of Al atoms in metal to oxide, N_{metal}/N_{oxide}, was 1.5, and the ratio of the IMFP of these electrons in oxide to metal, $\lambda_{oxide}/\lambda_{metal}$ was 2.6/2.8 [32]. From the equation, surface oxide thicknesses were calculated to be 3.39 nm for as-deposited Al and 7.32 nm for thermally-oxidized Al-O. For the further-annealed sample, since no Al metal signal was detected, the entire deposited Al layer (20 nm) was expected to be oxidized.

Composition and thickness determination of Al and Al-O films without Co catalyst were also studied using spectroscopic ellipsometry (SE; Figure 5(a)), and obtained model structures are summarized in Table 2: The optical models were constructed by Bruggeman

effective medium approximation (EMA) under the assumption that Al-O is transparent and has voids (pores) as its intrinsic properties [33]. Another assumption of the Bruggeman EMA theory is that small particles of different materials and different roughness can be intermixed [34]. Our modeling attempt for both samples was successful, with a very low mean square error (MSE) value calculated from the isotropic model. Consistent with the XPS results, as-deposited Al films were mainly constructed from the Al metal with thin native oxidized layer. For Al-T sample, model structure in Table 2 explains that 79 % (10.16 nm out of 12.90 nm) of unmixed Al metal remained, while the compositions of upper layers have the sequence of (Al + Al-O), Al-O, and (Al-O + void). Also, the top layer (Al-O + void) of further-annealed sample also showed an expansion in thickness, most probably due to the extra incorporation of oxygen after two heat treatments at 400 ^{o} C and 750 ^{o} C. Since amorphous alumina was reported to have higher thermal expansion coefficient than crystallized alumina, it is reasonable that the high porosity originates from amorphous Al-O [35].

From SE, the Al-O effective thicknesses for all samples were calculated by summing up independent Al-O layer and mixed layer (using the composition percentage of Al-O showed in Table 2). For example, in the case of thermally-oxidized sample, the Al-O total thickness was calculated from ((67 % x 2.87 nm) + (3.50 nm) + (38 % x 1.90 nm)), and the sum is equal to 6.14 nm. This calculation was also applied to as-deposited and further-annealed samples. For comparison, the results of Al-O effective thicknesses estimated by XPS and SE are summarized in Table 3 and plotted in Figure 5(b). From the plot, the changes in Al-O effective thickness obtained by XPS and SE analyses are completely consistent. Here, we hypothesize that the composition of Al-O increased after two different heat treatments. Thermal oxidation at 400 ^{o}C in air will not completely oxidize EB-deposited 20 nm Al metal films. It therefore can be suggested that Al-O of around 5 to 6 nm thickness produced after the thermal oxidation

and an increase to approximately 20 nm after being further annealing (750 ^{o}C) might be suitable for efficient VA-SWCNT growth using ethanol CVD.

Figure 7 shows the AFM tapping mode images of Al, Al-T, and further-annealed samples. For clarity, the differences of RMS surface roughness were plotted in Figure 7(e). The figures explain that even after two different heat treatments, the original surface roughness of the Al films did not drastically change. Compared to the uniform (mostly flat) surface of SiO_2/Si, the as-deposited Al surface is non-uniform, and the particles are clearly observable. Although the Co catalyst was not present on the samples surface, all samples showed relatively high surface roughness. The difference in RMS before and after those heat treatments is negligible, due to only a small deviation was confirmed. Even though it is possible that the presence of voids on Al-O films in the SE model might increase the RMS value, one should also consider the differences in particle size and films uniformity. Importantly, for non-uniform surface materials including Al-O, model approximation will be preferable with inclusion of voids during SE analysis. Voids used during SE analysis are not always defined as empty spaces of the sample surface, but can also as be pores or unoccupied crystal structures of the Al-O [32]. Hence, the AFM results agreed with the support layer advantages; distribution of smaller-size catalyst particles and high surface roughness to trap the catalyst into/on support layer surface for more active sites for CNT nucleation and growth.

4. Conclusion

The surface properties of Al-O films are important in order to understand their role in supporting catalyst particles for VA-SWCNT growth. Systematic studies on the properties of Al-O support layer used for VA-SWCNT growth were carried out. CNT growth efficiency is significantly depending on the preparation ways of Al-based support layer. From different Al-O films, thermally-oxidized Al-O has the most appropriate surface properties to support Co catalyst during ACCVD. The results suggested that low Al metal (or high Al oxide) composition ratio ($I_{metal}/I_{oxide} < 0.2$) and high RMS surface roughness (> 3 nm) of Al-O layers are essential for VA-SWCNT growth. Effective contact area and diffusion behavior of Co catalyst is strongly correlates to the surface roughness of support layer. And, significant variations in CNT growth results are also suggested to be due to the alteration of Co catalyst electronic structure caused by different Al-O surface chemical states.

From XPS *ex-situ* measurements, after further-annealed at CVD temperature (in Ar/H_2), the entire EB-deposited Al metal was completely-oxidized, Co transformed into small particles and partial reduction of Co oxide might have been occurred. Although Co could be re-oxidized due to atmospheric oxygen before XPS measurement, relative relation of Co oxidation states reveals the role of Co oxide as catalyst. Both Co oxide and metallic states are possibly essential for ethanol decomposition and CNT nucleation. Moreover, two different heat treatments at 400 and 750 ^{o}C produced different structural compositions of Al-O films. These heat treatments also did not affect the highly-roughened Al-O surface, but provided better Al and/or Al-O particle size distribution. Different morphology and surface chemical states of the support layer (in this work, Al-O) may cause variations in CNT growth performance.

Acknowledgments

This work was supported by a Grant-in-Aid from Japan Society for the Promotion of Science (JSPS) for Research Fellows. Part of this work was conducted in Kyoto Advanced Nanotechnology Network, supported by Ministry of Education, Culture, Sports, Science and Technology, Japan (MEXT). Special thanks to Mr. Daiki Hirose for sharing his expertise in spectroscopic ellipsometry. We also would like to thank Ms. Mary Ann Mooradian for the proof-reading and corrections of the manuscript.

References

[1] S. Maruyama, R. Kojima, Y. Miyauchi, S. Chiashi, M. Kohno, Chem. Phys. Lett. 360 (2002) 229.

[2] M. A. Mohamed, M. A. Azam, E. Shikoh, A. Fujiwara, Jpn. J. Appl. Phys. 49 (2010) 02BD08.

[3] M. A. Azam, M. A. Mohamed, E. Shikoh, A. Fujiwara, Jpn. J. App. Phys. 49 (2010) 02BA04.

[4] H. Sugime, S. Noda: Carbon 48 (2010) 2203.

[5] S. Maruyama, E. Einarsson, Y. Murakami, T. Edamura, Chem. Phys. Lett. 403 (2005) 320.

[6] H. Ohno, D. Takagi, K. Yamada, S. Chiashi, A. Tokura, Y. Homma, Jpn. J. Appl. Phys. 47 (2008) 1956.

[7] A-C. Dupuis, Progress in Materials Science 50 (2005) 929.

[8] P. B. Amama, C. L. Pint, S. M. Kim, L. McJilton, K. G. Eyink, E. A. Stach, R. H. Hauge, B. Maruyama, ACS Nano 4 (2010) 895.

[9] R. L. Vander Wal, T. M. Ticich, V. E. Curtis, Carbon 39 (2001) 2277.

[10] L. Delzeit, B. Chen, A. Cassel, R. Stevens, C. Nguyen, M. Meyyappan, Chem. Phys. Lett. 348 (2001) 368.

[11] H. Hongo, F. Niheya, T. Ichihashi, Y. Ochiai, M. Yudasaka, S. Iijima, Chem. Phys. Lett. 380 (2003) 158.

[12] S. Fan, W. Liang, H. Dang, N. Franklin, T. Tombler, M. Chapline, H. Dai, Physica E 8 (2000) 179.

[13] K. Hata, D. N. Futaba, K. Mizuno, T. Namai, M. Yumura, S. Iijima: Science 306 (2004) 1362.

[14] X. Wang, G-R. Han, Microelectron. Eng. 66 (2003) 166.

[15] N. Yao, G.Xiong, Y. Zhang, M. He, W. Yang, Catalysis Today 68 (2001) 97.

[16] S. Noda, K. Hasegawa, H. Sugime, K. Kakehi, Z. Zhang, S. Maruyama, Y. Yamaguchi, Jpn. J. Appl. Phys. 46 (17) (2007) L399.

[17] M. R. Alexander, G. E. Thompson, G. Beamson, Surf. Interface Anal. 29 (2000) 468.

[18] E. Einarsson, Y. Murakami, M. Kadowaki, S. Maruyama, Carbon 46 (2008) 923.

[19] R. Seidel, G. S. Duesberg, E. Unger, A. P. Graham, M. Liebau, and F. Kreupl, J. Phys. Chem. B 108 (2004) 1888.

[20] M. S. Dresselhaus, G. Dresselhaus, R. Saito, A. Jorio, Phys. Rep. 409 (2005) 47.

[21] M. A. Azam, A. Fujiwara, T. Shimoda, Abstract #1758, 219th ECS Meeting, The Electrochemical Society (2011).

[22] M. A. Azam, A. Fujiwara, T. Shimoda, J. New Mat. Electrochem. Systems 14 (2011) 173.

[23] R. Perrem, F. Henry, G. Peraudeau, B. Armas, R. Berjoan, J. Mater. Sci. 32 (1997) 1305.

[24] T. de los Arcos, Z. M. Wu, P. Oelhafen, Chem. Phys. Lett. 380 (2003) 419.

[25] D. Barreca, C. Massignan, Chem. Mater. 13 (2001) 588.

[26] J. Haber, L. Ungier, J. Electron Spectrosc. Relat. Phenom. 12 (1977) 305.

[27] N. S. McIntyre, D. D. Johnston, L. L. Coatsworth, R. D. Davidson, J. R. Brown, Surf.

Interface Anal. 15 (1990) 265.

[28] S. Oida, F. R. McFeely, and A. A. Bol, J. Appl. Phys. 109 (2011) 064304.

[29] S. Hofmann, R. Blume, C. T. Wirth, M. Cantoro, R. Sharma, C. Ducati, M. Havecker, S. Zafeiratos, P. Schnoerch, A. Oestereich, D. Teschner, M. Albrecht, A. Knop-Gericke, R. Schlogl, and J. Robertson, J. Phys. Chem. C 113 (2009) 1648.

[30] T. de los Arcos, M. G. Garnier, J. W. Seo, P. Oelhafen, V. Thommen, D. Arcos, J. Phys. Chem. B 108 (2004) 7728.

[31] M. Voß, D. Borgmann, G. Wedler, J. Catalysis 212 (2002) 10.

[32] B. Strohmeier, Surf. Interface Anal. 15 (1990) 51.

[33] D. E. Aspnes, Thin Solid Films 89 (1982) 249.

[34] A. Franquet, J. De Laet, T. Schram, H. Terryn, V. Subramanian, W. J. van Ooij, J. Vereecken, Thin Solid Films 384 (2001) 37.

[35] A. M. Huntz, L. Marechal, B. Lesage, R. Molins, Appl. Surf. Sci. 252 (2006) 7781.

Figure & Table captions

Figure 1. (Color online) (a) AFM-tapping mode topography and 3D images and
(b) XPS analysis of 20 nm as-deposited Al films, oxidized samples from different oxidation methods, and as-deposited alumina. As labeled in the figure, Al 2p oxide and metal peaks are represented by blue and red lines, respectively. The calculated I_{metal}/I_{oxide} ratios are shown on the right side of the figure.

Figure 2. (a) SEM images of CNTs grown using ACCVD process at t = 10 min and T_{CVD} = 750 ^{o}C using Co and different support layers. Note that for clarity, Al and alumina are tilted to 45 ^{o}, and Al-T, Al-UV, Al-P are cross-sectional images. Display scales of all samples are also different. (b) Relation between CNT growth results and RMS surface roughness for all samples.

Figure 3. (a) SEM images of CNTs grown using ACCVD process at t = 10 min, T_{CVD} = 750 ^{o} C. The images were taken from above of the substrate, cross-sectional, and a close-up (high resolution) from the cross-sectional image. (b) Raman spectrum of CNTs grown from Co/Al-T/SiO_2/Si substrate.

Figure 4. (Color online) (a) XPS survey spectra of Co/Al-T (top), Al-T sample without Co (middle), and SiO_2/Si substrate as reference (bottom).
(b) Narrow XPS spectra of O 1s and Al 2p regions for Al, Al-T, and further-annealed samples. Main (Al 2p oxide and metal) peaks are represented by blue and red lines, respectively. The calculated I_{metal}/I_{oxide} ratios are shown on the right side of the figure.
(c) Samples coated with 0.5 nm Co catalyst. Note that asterisks * represent the shake-up satellite peaks of Co 2p.

Figure 5. (Color online) (a) ψ plots depending on the wavelength (λ = 350 – 1000 nm),

measured at incidence angle 75 ^{o}. Note that the figures are sequenced from the bottom (Al) to the above (further-annealed). (b) A plot of Al-O effective thickness for differently prepared samples.

Figure 6. (Color online) AFM tapping mode images of (a) SiO_2/Si substrate, (b) as-deposited 20 nm Al films, (c) Al-T, and (d) further-annealed. The scan area was (1 x 1) μm^2 and (e) a plot comparing RMS surface roughness of (a) – (d).

Table 1. Surface properties of different support layers, measured by AFM, XPS and CNT growth results. Sample Al, Al-T, Al-UV, Al-P were fabricated from 20 nm pure Al metal. In contrast, alumina films (20 nm) were directly-deposited, without further oxidation process. I_{metal}/I_{oxide} ratios were calculated from XPS intensities of Al 2p region. AFM and XPS analyses were performed without the deposition of Co catalyst. VA-CNT growth results were obtained using SEM.

Table 2. Model structure obtained by Bruggeman EMA model for as-deposited Al 20 nm (Al), thermally-oxidized Al-O (Al-T), and further-annealed samples. The samples are sequenced from the bottom (Al) to the above (further-annealed). And, the compositions of each layer for all samples are sequenced from top (surface) to bottom of the samples structures. Also, the SiO_2 thicknesses of 402.39 nm (Al, Al-T) and 399.51 nm (further-annealed) were used during fitting process of the model approximation. Similar heat treatments were performed for blank SiO_2/Si substrate, and the above-mentioned SiO_2 thicknesses were obtained after SE measurement.

Table 3. Comparison of Al-O effective thicknesses (estimated using XPS and SE) for as-deposited Al films, thermally-oxidized Al-O, and after further annealing at 750 ^{o} C. Note that the samples are sequenced from the bottom (Al) to the above (further-annealed).

Figure 1(a)

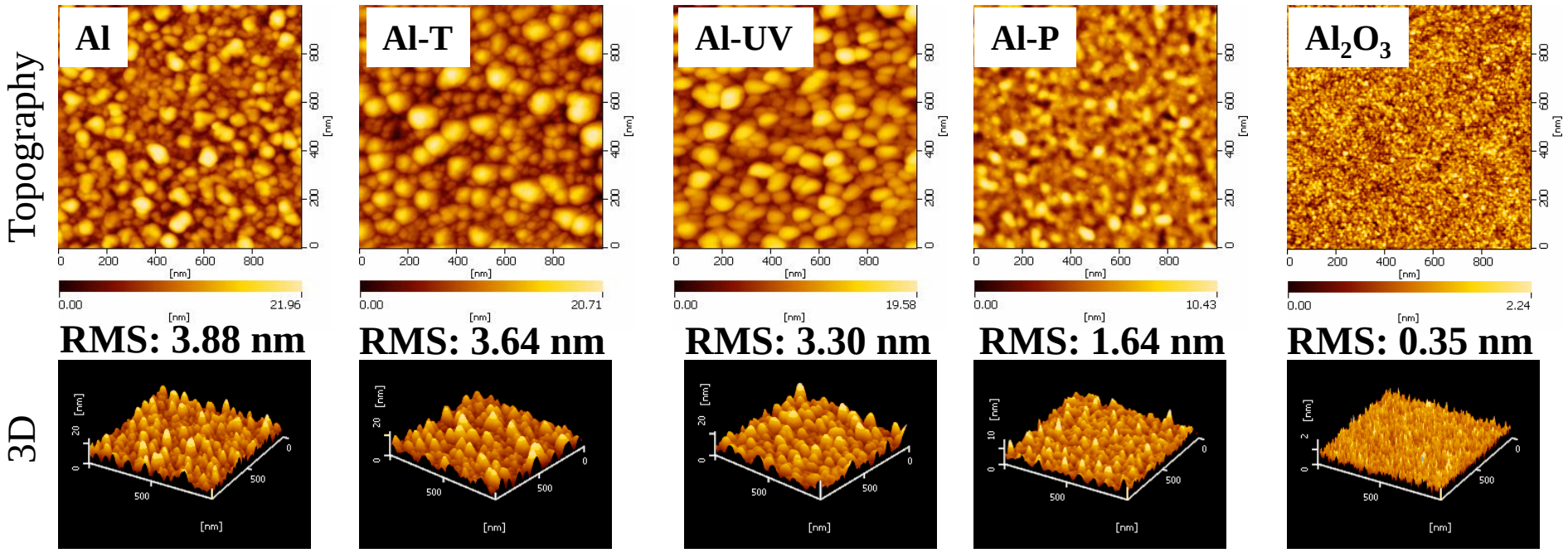
Topography
Al
Al-T
Al-UV
Al-P
Al2O3
RMS: 3.88 nm
RMS: 3.64 nm
RMS: 3.30 nm
RMS: 1.64 nm
RMS: 0.35 nm
3D

Figure 1(b)

Different Al-based support layers

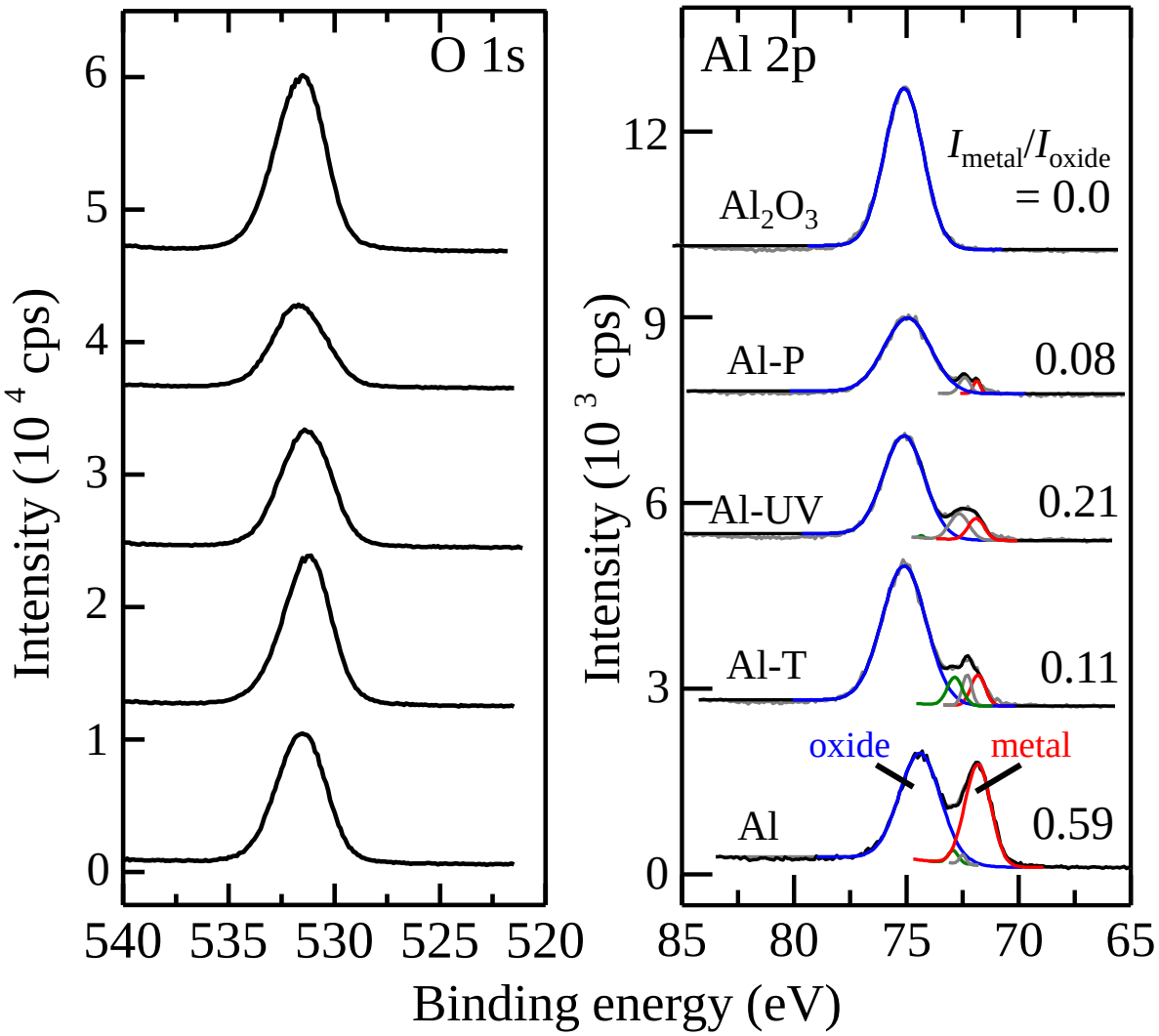

Figure 2(a)

Al	Al-T	Al-UV	Al-P	Al_2O_3
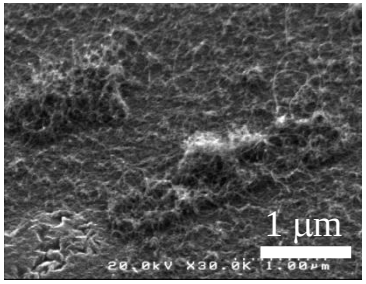	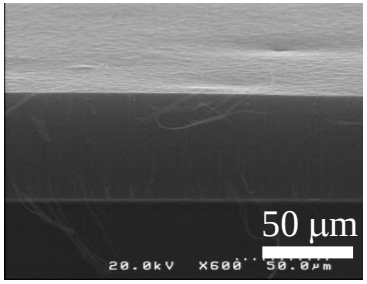	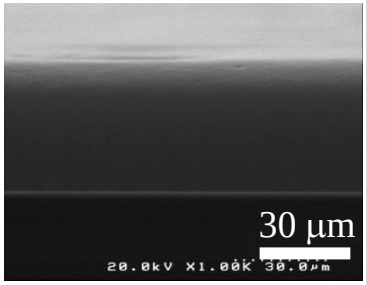	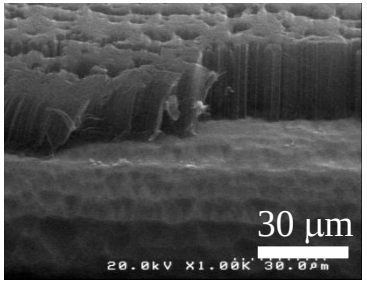	

Note that for clarity:

1. *Al, Al_2O_3: Tilted to 45 ^{o}.*
2. *Al-T, Al-UV, Al-P: Cross-sectional.*
3. *Display scales of all samples are different.*

Figure 2(b)

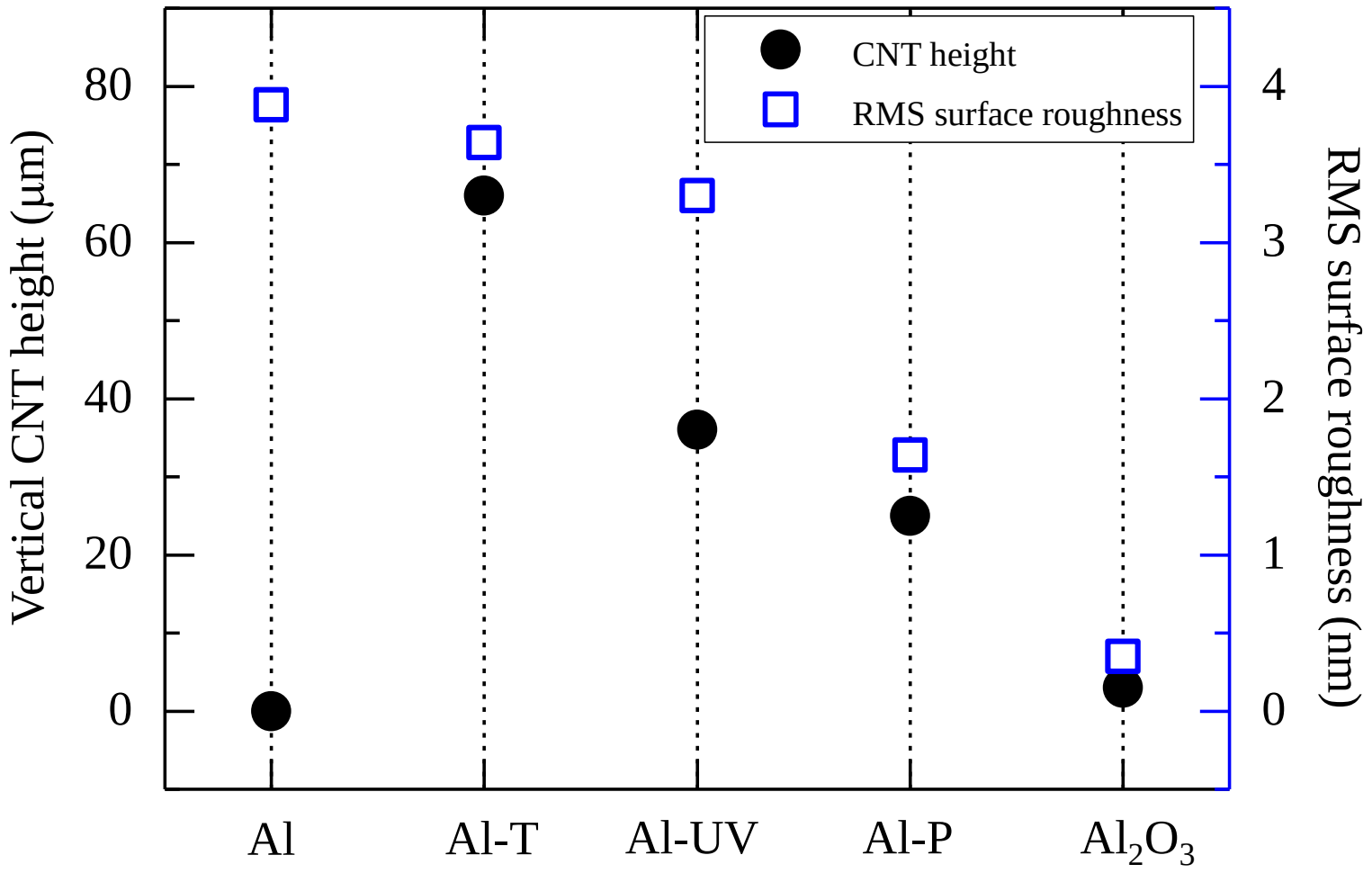
CNT height
RMS surface roughness
Vertical CNT height (μm)
RMS surface roughness (nm)
0
20
40
60
80
0
1
2
3
4
Al
Al-T
Al-UV
Al-P
Al2O3

Figure 3(a)

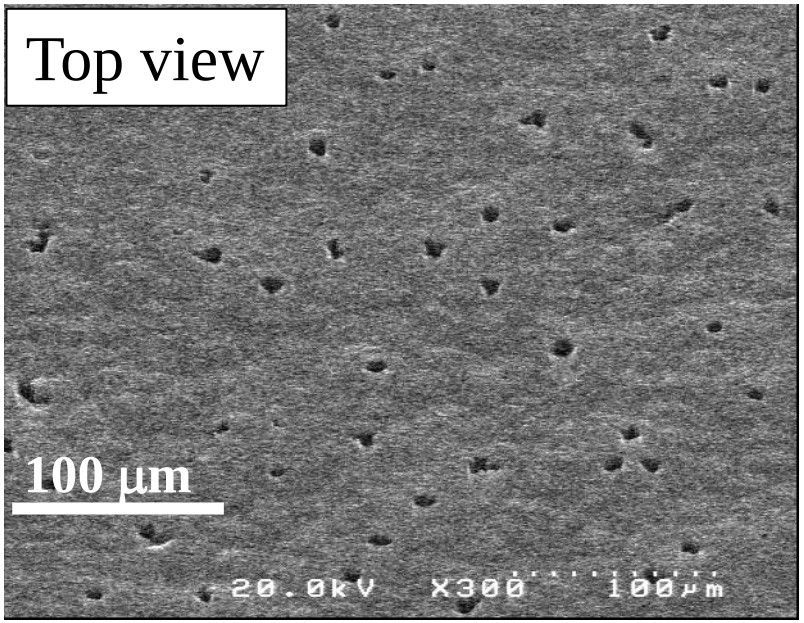
Top view
100 μm
20.0kV X300 100μm

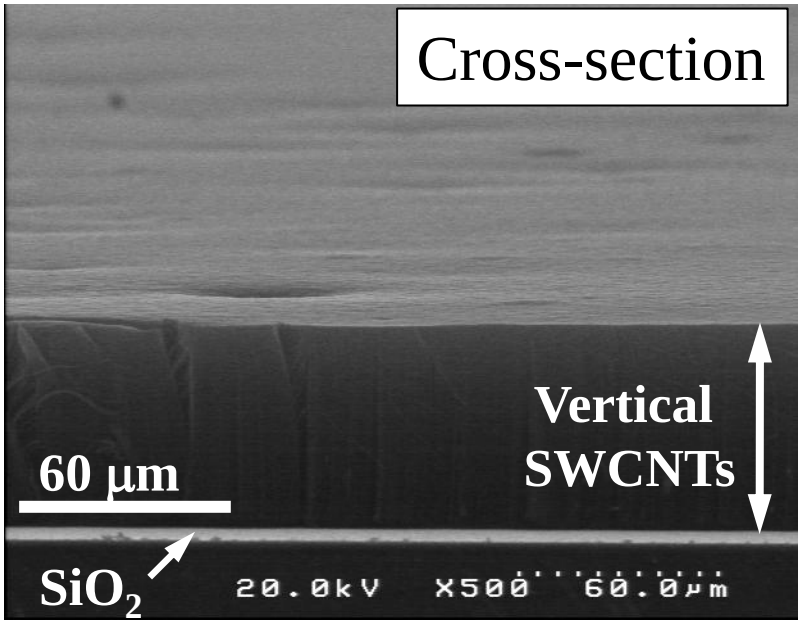
Cross-section
Vertical
SWCNTs
60 μm
SiO2
20.0kV X500 60.0μm

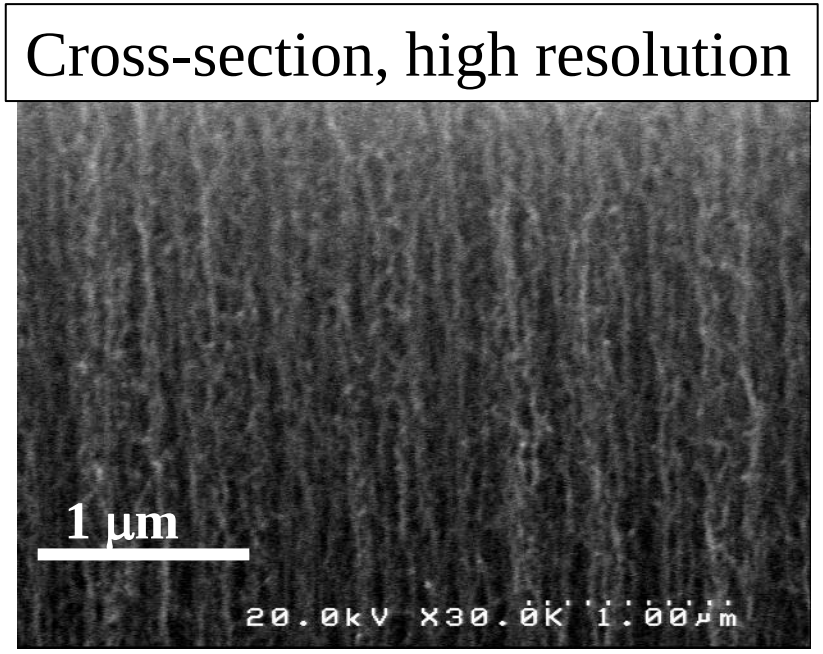
Cross-section, high resolution
1 μm
20.0kV X30.0K 1.00μm

Figure 3(b)

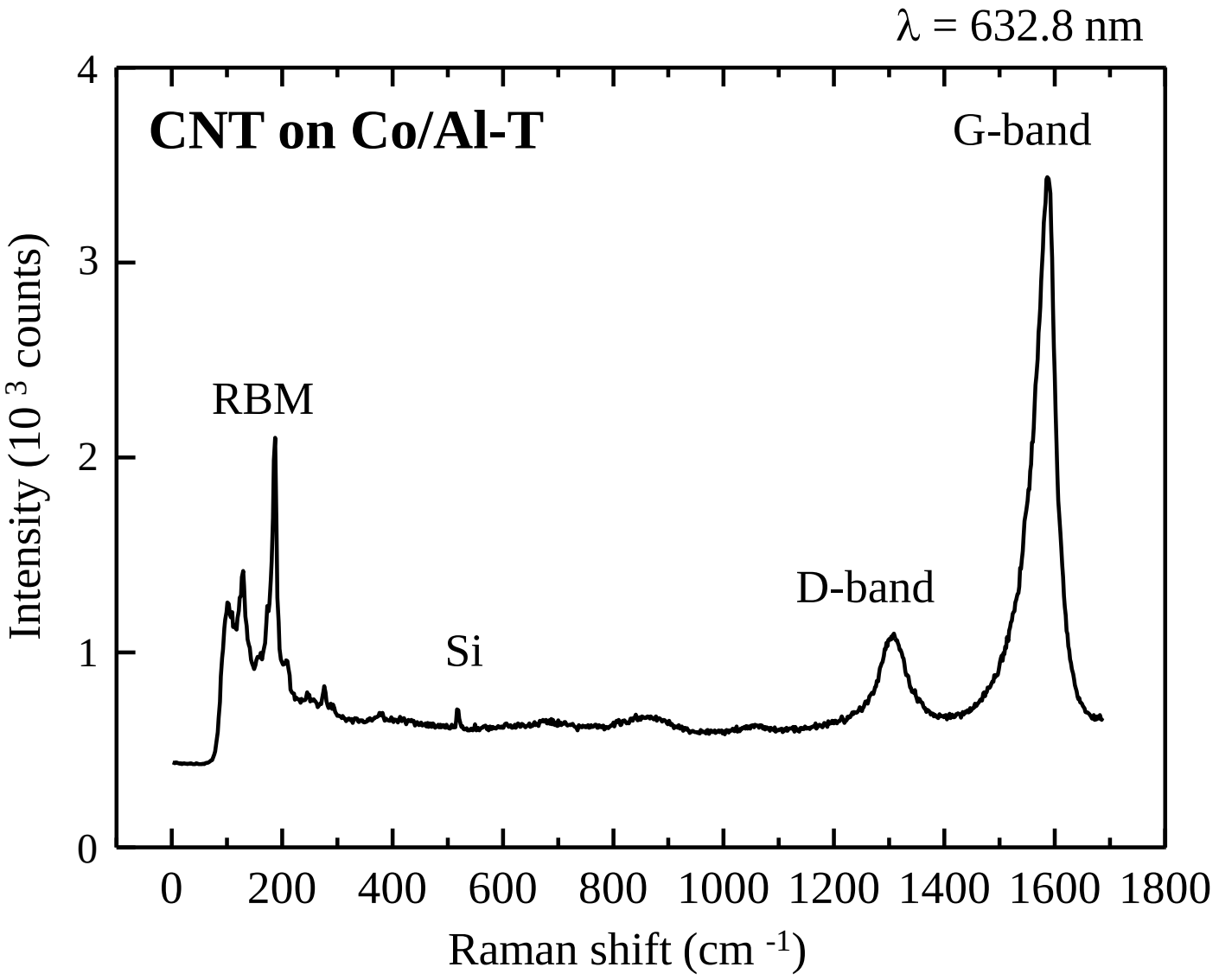
λ = 632.8 nm
CNT on Co/Al-T
G-band
RBM
D-band
Si
Intensity (10 3 counts)
Raman shift (cm -1)
0
1
2
3
4
0
200
400
600
800
1000
1200
1400
1600
1800

Figure 4(a)

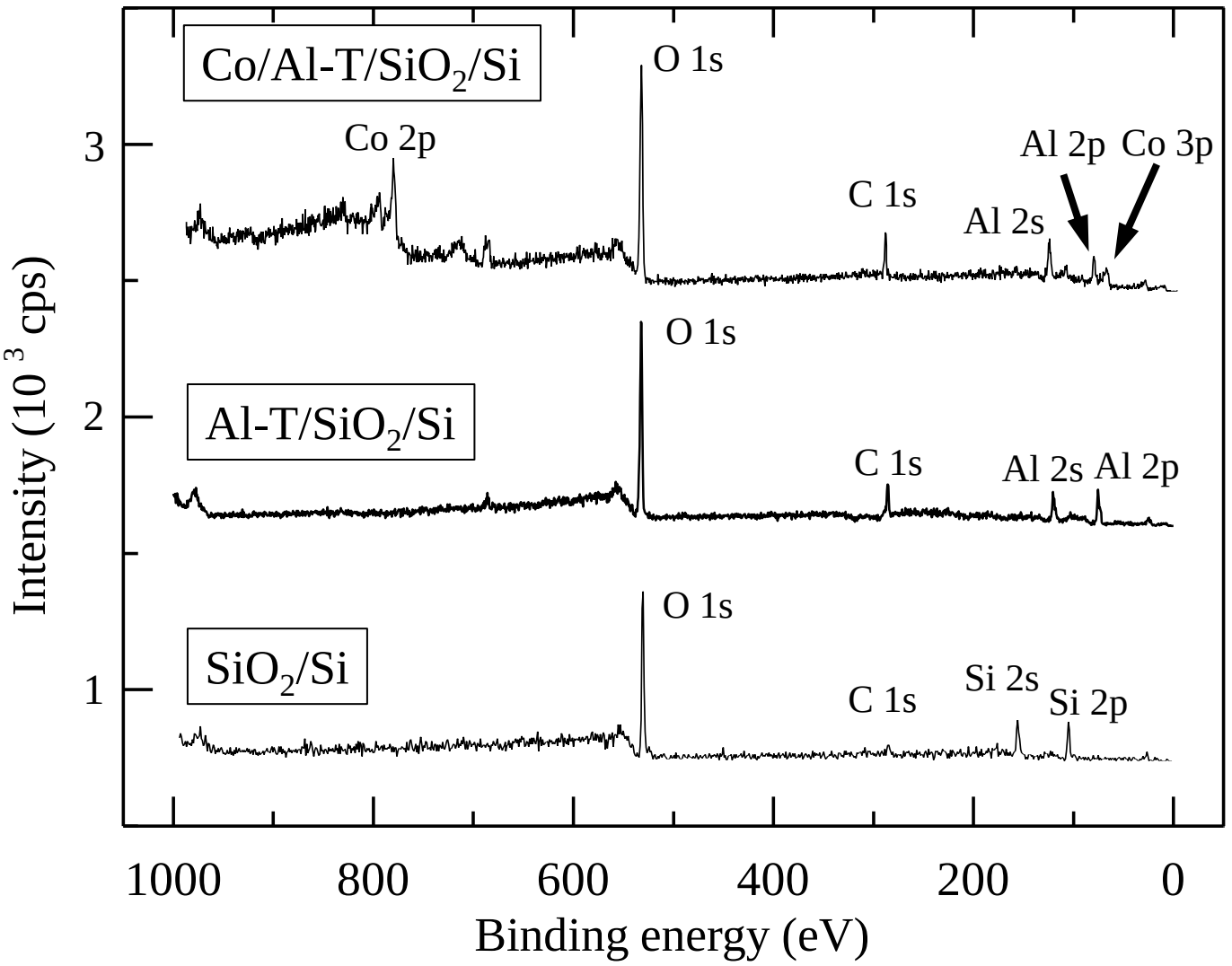
Co/Al-T/SiO2/Si
O 1s
Co 2p
Al 2p
Co 3p
C 1s
Al 2s
Al-T/SiO2/Si
O 1s
C 1s
Al 2s
Al 2p
SiO2/Si
O 1s
C 1s
Si 2s
Si 2p
Intensity (10 3 cps)
3
2
1
1000
800
600
400
200
0
Binding energy (eV)

Figure 4(b)

XPS: Al-T (without Co)

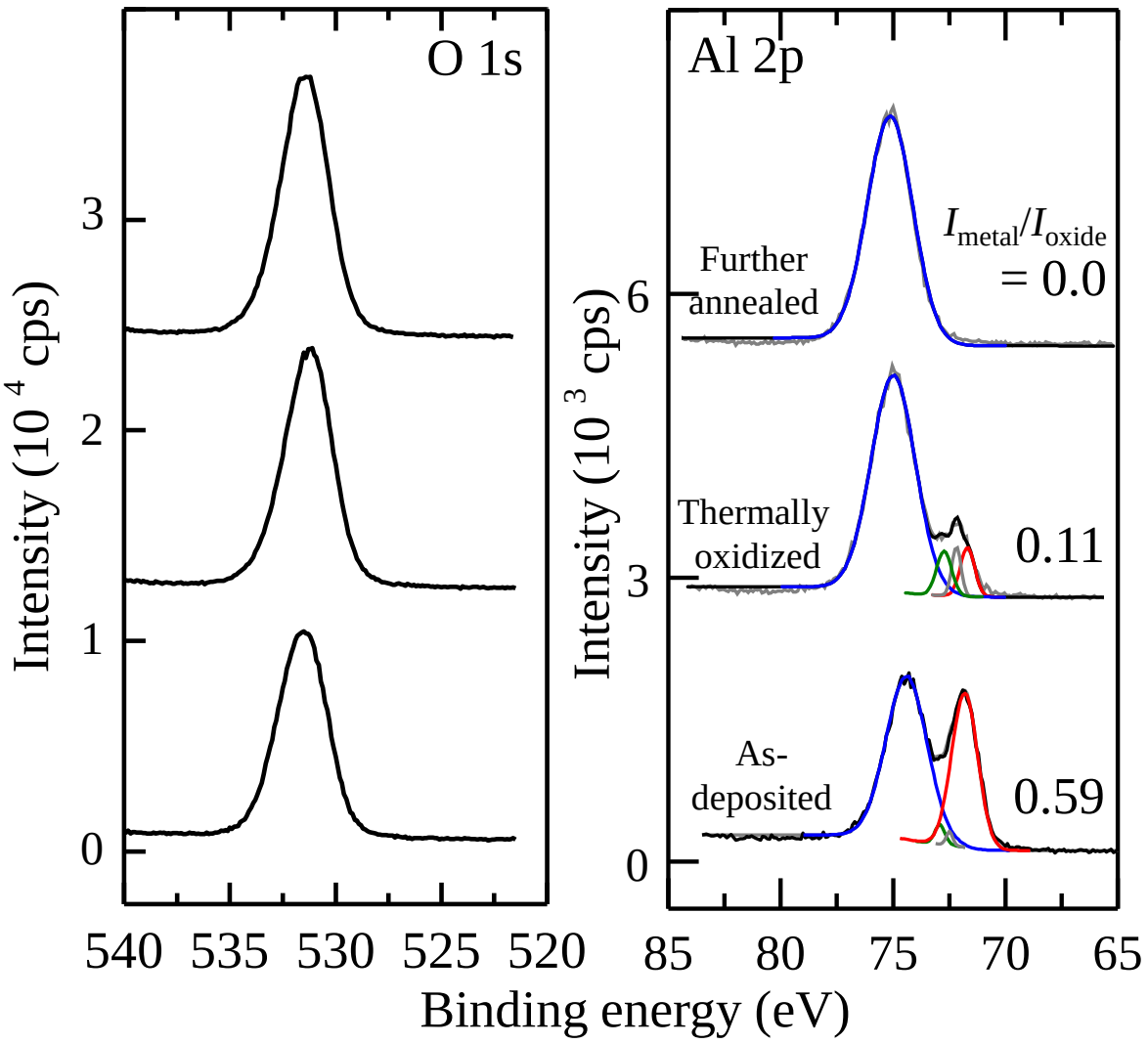

Figure 4(c)

XPS: Co/Al-T

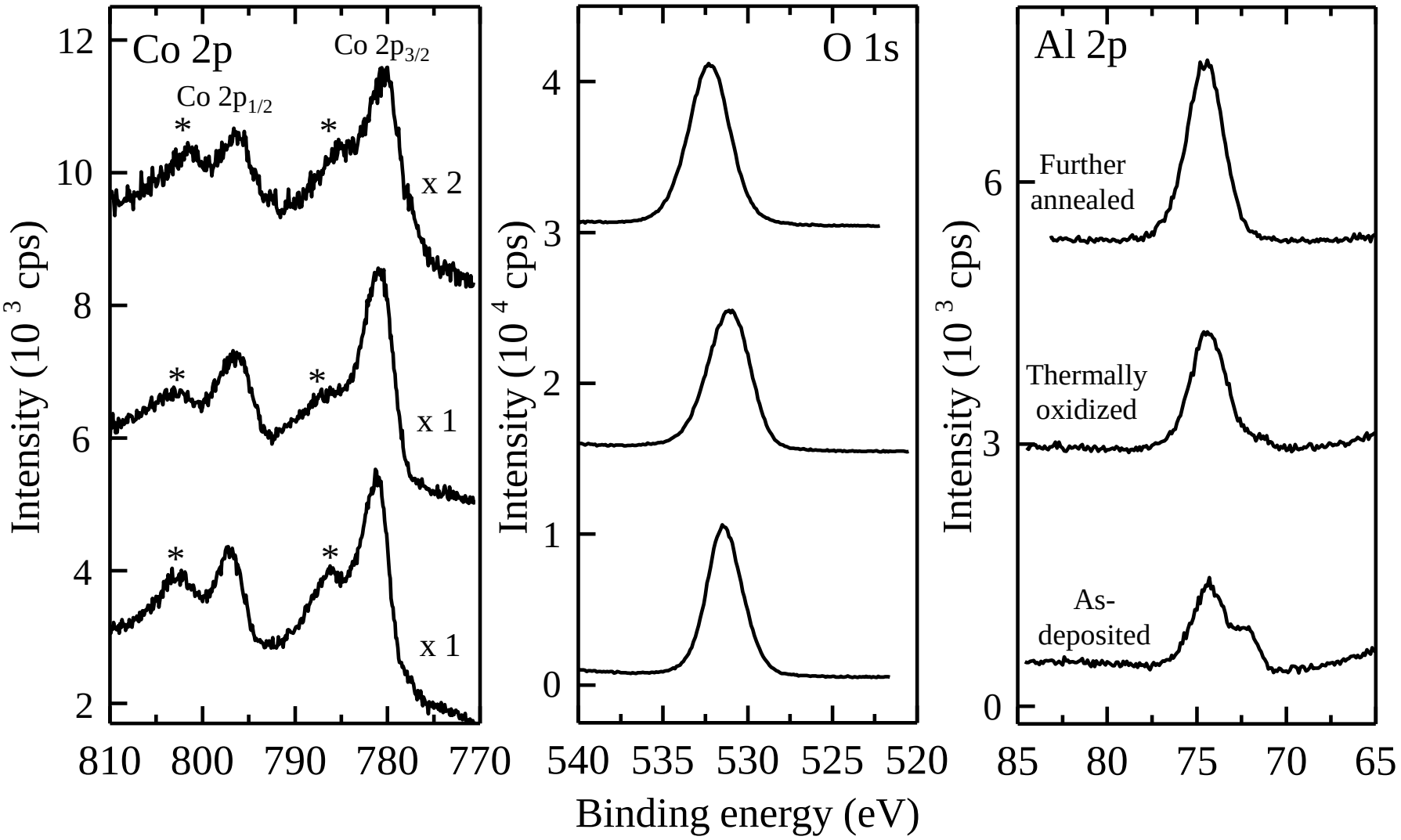

Figure 5(a)

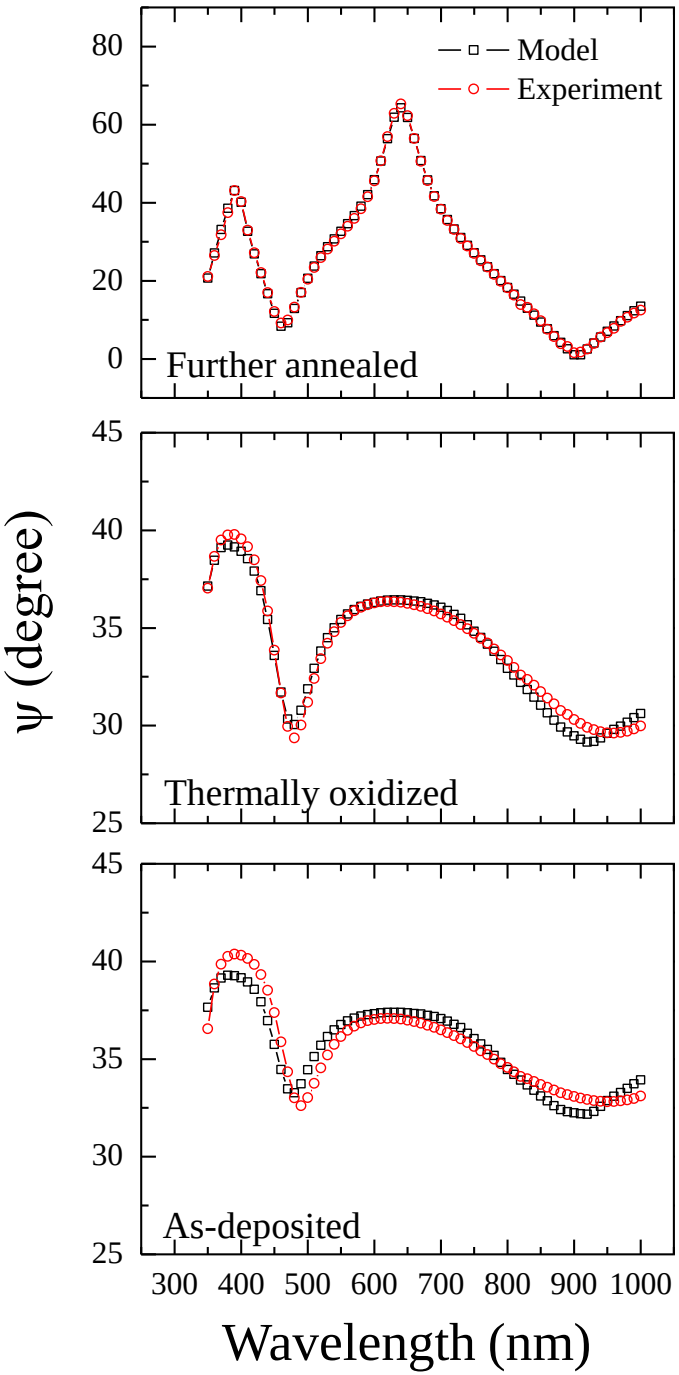
Model
Experiment
Further annealed
Thermally oxidized
As-deposited
ψ (degree)
Wavelength (nm)
80
60
40
20
0
45
40
35
30
25
300
400
500
600
700
800
900
1000

Figure 5(b)

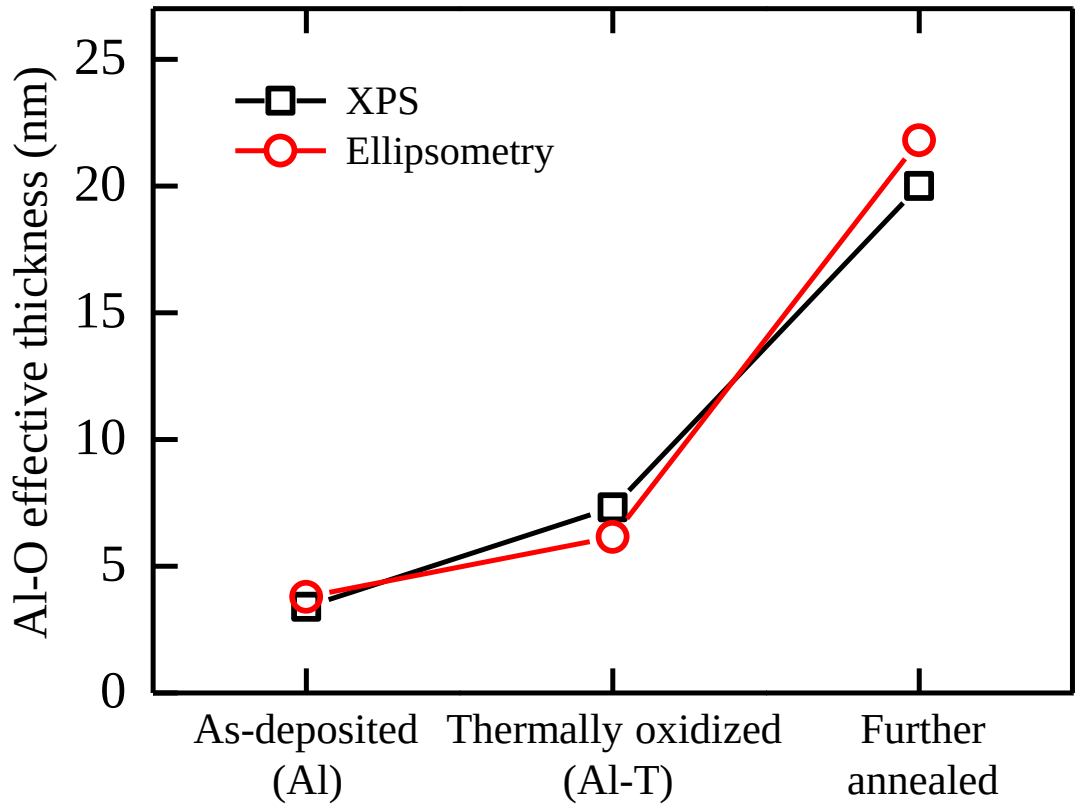
Al-O effective thickness (nm)
25
20
15
10
5
0
XPS
Ellipsometry
As-deposited
(Al)
Thermally oxidized
(Al-T)
Further
annealed

Figure 6

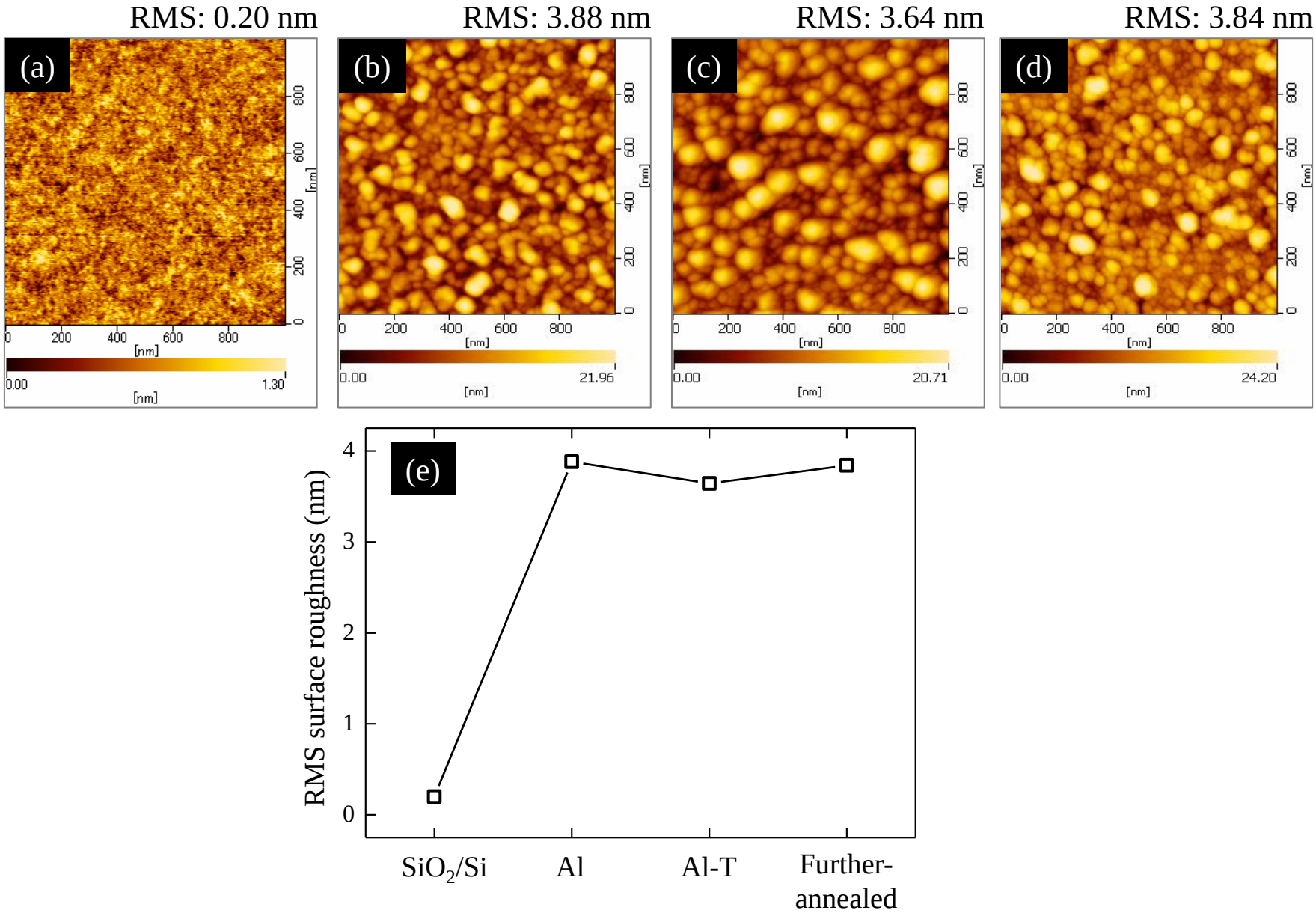
RMS: 0.20 nm
RMS: 3.88 nm
RMS: 3.64 nm
RMS: 3.84 nm
(a)
(b)
(c)
(d)
(e)
0.00
1.30
21.96
20.71
24.20
[nm]
RMS surface roughness (nm)
SiO2/Si
Al
Al-T
Further-annealed

Table 1

Methods to produce Al-O	Sample name (label)	AFM		XPS	ACCVD
		RMS roughness (nm)	Grain size (nm)	Al 2p I_{metal}/I_{oxide}	VA-CNT height (μm)
As-deposited Al metal (no post-treatment)	Al	3.88	17.5	0.59	0
Thermal oxidation (400 ^{o}C, air)	Al-T	3.64	18.0	0.11	66
UV ozone oxidation (60 min)	Al-UV	3.30	14.0	0.21	36
Plasma oxidation (30 W, 10 min, 50 sccm)	Al-P	1.64	9.0	0.08	25
As-deposited alumina (no post-treatment)	Alumina	0.35	1.5	0	3

Table 2

	Composition	Thickness (nm)	Total thickness (nm)	MSE
Further-annealed	Al-O (71%) + Al (9%) + Void (20%)	30.70	30.87	18.52
	Al	0.17		
Thermally-oxidized (Al-T)	Al-O (38%) + Void (62%)	1.90	18.43	10.75
	Al-O	3.50		
	Al (33%) + Al-O (67%)	2.87		
	Al	10.16		
As-deposited (Al)	Al-O	2.70	18.9	14.05
	Al (67%) + Al-O (33%)	3.30		
	Al	12.9		

Table 3

	Effective thickness of Al-O (nm)	
	XPS (Equation 1)	SE (Table 2)
Further-annealed	≈ 20	21.80
Thermally-oxidized (Al-T)	7.32	6.14
As-deposited (Al)	3.39	3.79